

Environment–Vehicle Interaction Modeling for Unmanned Aerial System Operations in Complex Airflow Environments

Brian E. McGrath, Bohdan Z. Cybyk, and Timothy M. Frey

Existing unmanned aerial system (UAS) platforms do not perform well in environments with complex terrain and highly variable aerodynamics. However, it is essential that the warfighter operate UASs in such complex environments (e.g., urban areas, canyons, and mountains). Thus, a need exists for a high-fidelity, physics-based modeling and simulation framework addressing this parameter space. The APL UAS mission planning and simulation tool provides the framework to perform environment–vehicle interaction studies. The framework includes computational fluid dynamics modeling of the complex terrain airflows, vehicle aerodynamics and dynamics models, terrain models, and a visualization engine. This article focuses on development, formulation, and implementation, within this framework, of environment–vehicle interaction models for UAS operations in complex environments. Results for implementation of one environment–vehicle interaction model show the effects on the trajectory (e.g., latitude, longitude, altitude, vehicle attitude, vehicle rates, and autopilot control commands). Examination of such results helps understand the effects of these interaction models in the context of validated terrain airflow models in realistic complex environments. The APL UAS mission planning and simulation tool provides a compelling synthetic environment in which to perform these environment–vehicle interaction studies that includes relevant operational constraints to increase the probability of mission success for UAS operations in these complex environments.

INTRODUCTION

Today's warfighters must face their adversaries within a constantly changing and challenging battlefield envi-

ronment. To help counteract these new threats, our military is deploying ever-increasing numbers of unmanned

aerial systems (UASs), the use of which creates significant advantages for warfighters. These advantages include the ability to perform autonomous intelligence, surveillance, and reconnaissance as well as close-in strike missions without putting the warfighter directly in harm's way. Our adversaries are constantly changing tactics, techniques, and procedures and are highly mobile, necessitating that our warfighters have a persistent set of "eyes in the sky" to help identify, understand, and react to these changes. The battlefield itself is another changing and challenging environment. Often the warfighter faces the prospect of engaging the adversary in both clear and adverse weather conditions within highly complex terrain, including geographic landscapes like urban areas, canyons, mountains, and heavily wooded settings. Thus, there is a need to plan mobile and non-mobile target engagement missions in these settings.^{1,2}

Existing UASs do not easily lend themselves to operation within complex and highly variable aerodynamic environments. Whether the warfighter performs autonomous or nonautonomous UAS operations, the complexity of the airflow through these terrains affects the stability and control of the UAS mainly because of the highly variable wind gusts. The stability and control concerns, in turn, can constrain operator visibility and communication effectiveness, increasing overall mission risk. Consequently, the UAS must possess the inherent ability to maintain stability and control for basic flight maneuvers despite wind changes, weather variability, and communication loss yet respond quickly and effectively to dynamic conditions on the ground. In essence, the UAS autopilot should be robust enough to allow for autonomous operation within these complex flight environments.

Understanding the close coupling between the vehicle and the dynamic environment through which it is flying is paramount to defining the control authority and autopilot robustness required for UAS operations

and mission success. Thus, a detailed understanding of the time-varying airflow and its impact on vehicle performance is a prerequisite to reducing overall risk of mission failure. The primary influence on UAS flight stability and control is the effect of the wind. Although the linear velocity effects of the wind are straightforward, the rotational effects of the wind are not. These rotational effects can be significant and important for UAS stability and control, and thus autopilot robustness. The geometric size and mass of the UAS vehicle determines the magnitude and importance of the rotational effects within these complex environments. In many modeling and simulation (M&S) applications, these rotational effects are often overlooked or neglected because of their complexity; hence, the resultant performance predictions are potentially inaccurate.

To begin to understand the underlying complexity of airflows within these complex environments, consider a cube—a single parameter representation that approximates one of many buildings in an urban environment. Experimental studies³ have confirmed that the structure of the airflow past a surface-mounted cube (Fig. 1) is sensitive to both the upstream velocity and surface plate boundary conditions. The complexity of the flow around a single cube is illustrated in Fig. 1. Shown in the figure are multiple variable-length and time-scale vortices, recirculation regions, and separation and reattachment lines.³ One can easily deduce that as the urban geometry increases in complexity (e.g., multiple cubes of various sizes and spacings), the complexity of the associated airflows increases as well. Buildings in close proximity to one another shed vortices with large dynamic recirculation zones, directly affecting local airstreams. Additional complexity is added by the presence of varying meteorology, a stratified atmospheric boundary layer, and vertical shears created by solar heating and cooling. All of these considerations substantiate the complexity of urban airflows;^{4,5} other complex environments are analogous.

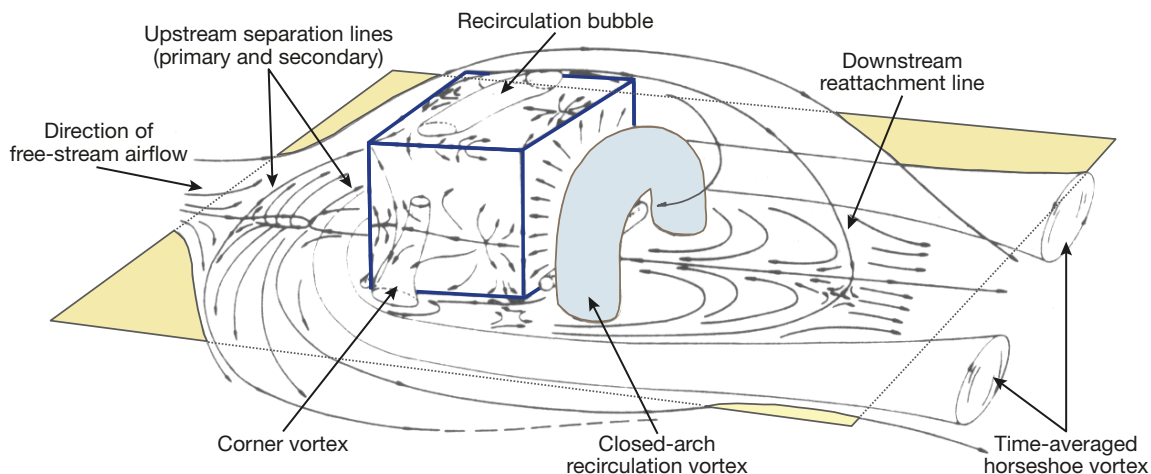


Figure 1. Representative airflow over a single surface-mounted cube. (Reprinted with permission from Ref. 3, ©1993, ASME.)

A key to successful UAS flight in these challenging airflow environments is the fundamental understanding of parametric relationships that dominate urban aerodynamics. Some of these parameters are geometric similarity, intensity of environment turbulence, turbulence length scales, surface roughness, Reynolds number (ratio of the fluid inertia forces to viscous forces), and Richardson number (ratio of thermally produced turbulence to turbulence generated by vertical shear). Traditionally, a combination of controlled wind tunnel experiments, field trials, and modeling would be used to underpin UAS technology development programs for less complex environments. However, engineers face significant challenges and obstacles in attempting to understand and model the dominant physics within more complex terrains. Laboratory experiments and field trials can provide useful data on modeling the aerodynamic interactions but lack the environmental control needed for accurate model validation. Furthermore, they are prohibitively expensive or logistically impossible for many scenarios. Wind tunnel testing could facilitate model validation through controlled, repeatable experiments with well-characterized inflow conditions. However, wind tunnel testing simply cannot match the flow conditions required at the geometric subscale sizes for the complex terrains (e.g., the Reynolds number). Another limitation of wind tunnel testing can be attributed to the neglect of atmospheric and thermal stratification effects. Because of these shortcomings, high-fidelity, physics-based computational methods are examined and applied to model the aerodynamics within the complex terrain environment.

One such computational method is the large eddy simulation (LES). A form of computational fluid dynamics, LES can capture the geometric definition of the complex terrain environments with varying wind directions, varying meteorological conditions, atmospheric boundary layer stratification, and vertical shear. LES solutions can be used to provide the aerodynamics (or winds) for a given complex terrain to a UAS trajectory simulation tool. By having a UAS “fly” through realistic numerical wind environments, trajectory simulations can be used to define UAS stability and control authority requirements needed to design robust autopilots that maintain controllable flight.

As mentioned earlier, one aspect of particular interest is the relationship between controllability and the rotational interaction effects imparted by wind onto the UAS vehicle. By using the computational LES database of the complex terrain environment, environment–vehicle interaction models of the wind rotational effects can be developed. Physics of the environment–vehicle interaction that can be modeled are the wind rotational velocity, angular momentum, and/or moments imparted onto a UAS vehicle during a flight or mission.

The Johns Hopkins University Applied Physics Laboratory (APL) has developed a UAS mission planning and simulation tool underpinned by a rigorous physics-based, five-component M&S framework to tackle the complex terrain and urban environment problem.^{6,7} The motivation behind the creation of this UAS simulation tool is the need to not only understand the physics of each component-level phenomenon but also to accurately capture the interactions of these phenomena in an end-to-end environment.

This article focuses on the model development for the interactions between the complex terrain airflow environment and the UAS flying through it. These environment–vehicle interaction models are critical to assessing the performance of a representative UAS platform “flying” through a highly turbulent urban environment. Five separate environment–vehicle interaction models of the wind rotational effects have been formulated. These models are categorized into two designations, namely coefficient-based or rate-based, depending on whether the model is applied on the left-hand or right-hand side of the equations of motion, respectively. Regardless of model designation, certain information must be known, *a priori*, about both the vehicle aerodynamic characteristics and environment airflow. For the rate-based models, information must be known for the UAS geometry and mass properties as well as the airflow within the complex terrain environment. While this same information must be known for the coefficient-based model, a thorough definition of the UAS aerodynamic coefficients must also be known as a function of the various flight parameters (e.g., velocity, angles of attack and sideslip, and control surface deflection angles). These environment–vehicle interaction models vary in the level of physics captured and implementation simplicity. They are implemented in the UAS vehicle dynamics component of the UAS mission planning and simulation tool.

UAS MISSION PLANNING AND SIMULATION TOOL

The APL UAS mission planning and simulation tool accurately captures the primary physics interactions not only on a component level but also from an end-to-end systems engineering perspective. It is often the case that systems engineering is executed in a piecemeal fashion, and as such, subsystems or component interactions within and external to the overall system are not fully understood until the system is near completion. This often results in painful lessons learned too late in the process, at a time when the cost of change is prohibitively high. The M&S framework is modular in design so that various components can be interchanged as the UAS vehicle and/or the terrain and associated airflow environment change for a given mission. The five components of the framework consist of the unsteady LES

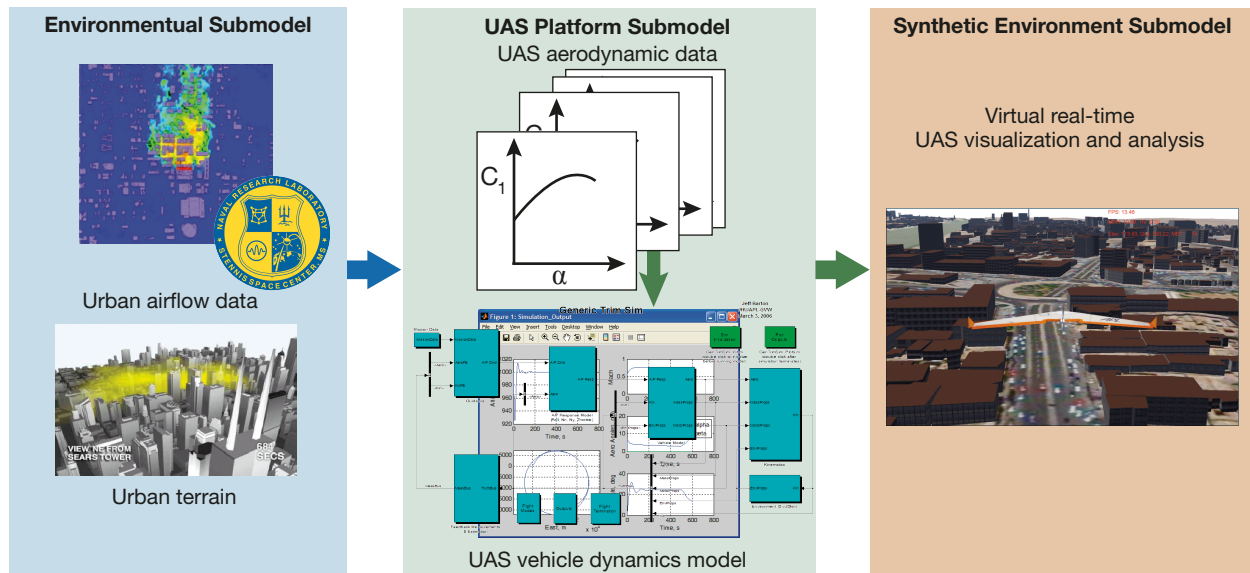


Figure 2. Components and submodels of the UAS mission planning and simulation tool. (Adapted from Ref. 7 with permission of the American Institute of Aeronautics and Astronautics.)

terrain airflow database, the complex terrain, the UAS aerodynamic database, the UAS vehicle dynamics, and a synthetic modeling environment. The five components are grouped into three major submodels: the environmental submodel, the UAS platform submodel, and the synthetic environment submodel (Fig. 2).

Environmental Submodel

The environmental submodel comprises everything necessary to model the environment in which the UAS will operate, including the complex terrain, terrain airflow models, and communications. The complex terrain must not only accurately represent elevation, structures, and other topographical features, but it must also contain data about its fundamental properties to support potential sensor modeling. As an example, a lidar pulse interacts differently with a glass building than with a concrete bridge; thus these texturing features must be included. For accurate communications modeling, factors such as line of sight, propagation loss, refraction, radio type, and encryption protocols are critical to mission success of the UAS within these complex terrain environments.

UAS Platform Submodel

The UAS platform submodel integrates elements of the vehicle aerodynamics, flight dynamics, and terrain airflow data to capture the basic vehicle motion coupled with the environment-vehicle interactions. It also captures specific control algorithms for the UAS platform, other subsystems that make up the UAS platform (e.g., power, navigation), and payloads (e.g., sensors). Challenges in the UAS platform submodel revolve around understanding the level of fidelity necessary for each subsystem.

Synthetic Environment Submodel

The synthetic environment submodel is the wrapper that integrates both the environmental and UAS platform submodels into an end-to-end analysis framework that handles synchronization of data, interoperability of M&S components, and overall scenario control. In addition, the synthetic environment provides the visual component of complex terrain and UAS platform. This visualization feature results in a tool useful for mission planning, training, and analysis. Because of the potential complexity of UAS missions, the high numbers of entities involved (e.g., UAS, ground sensors, warfighters, etc.), and the number of variables that correlate with mission success or failure, the ability to visualize everything that is happening in a given scenario gives operators and analysts an ability to synthesize data and draw conclusions that would never be apparent from engineering plots alone.

A snapshot from the synthetic environment model, for a simulation centered in downtown Baghdad and involving the use of the Unicorn UAS (made by Procerus Technologies), is shown in Fig. 3. The downtown Baghdad airflow environment is simulated by an LES computational fluid dynamics method, and the Unicorn UAS “flies” through this environment following a prescribed path. Paramount to the M&S framework is the modularity feature mentioned above. Much of the power of this M&S framework and systems engineering approach derives from the ability to quickly exchange components (e.g., terrain airflow database, complex terrain, UAS aerodynamics database, and UAS vehicle dynamics) to perform mission trajectory trade studies and analysis of alternatives in an end-to-end synthetic modeling environment. As mentioned above, two of the



Figure 3. Snapshot from the UAS mission planning and simulation tool. (Reprinted from Ref. 7 with permission of the American Institute of Aeronautics and Astronautics.)

critical pieces of the UAS M&S puzzle are the complex terrain airflow dynamics and the interactions between the UAS and the complex terrain airflow. The following two subsections provide a detailed description of the environment–vehicle interaction models.

Unsteady LES Terrain Airflow Database and Complex Terrain Components

The critical pieces of the environment submodel are the modeling of the urban and complex terrains and the airflow through these terrains. These pieces provide wind data from which the interactions between the environment and vehicle can be determined. Thus, the development and application of these environment–vehicle interaction models depends significantly on accuracy of the representation of these terrains and airflow through them. In recent years, computing the airflow in urban and complex terrains has played an important role in other applications, particularly urban aerodynamics and the prediction of contaminant transport within the urban landscape.^{5,8–10} Leveraging the computational tools used for modeling contaminant transport helps advance the development of the environment–vehicle interaction models, as well. At the present time, LES provides the best combination of accuracy and efficiency for urban aerodynamics simulation. LES simulations are able to capture significant flow unsteadiness, localized vortex shedding, and the wide range of large-scale to small-scale unsteady flow features governing the urban environment.

Given the potential for higher computational efficiency, the Monotone Integrated LES (MILES) approach^{11,12} is well suited for urban landscape scenarios. The MILES approach is used in the current application with the FAST3D-CT 3-D urban aerodynamics model based on the scalable, low-dissipation, flux-corrected transport convection algorithm.¹⁰ The relevant physical processes simulated in FAST3D-CT include complex

building vortex shedding; flows in recirculation zones, with algorithms approximating the dynamic subgrid-scale turbulence and stochastic backscatter; a stratified urban boundary layer with realistic wind fluctuations; solar heating including shadows from buildings and trees; aerodynamic drag and heat losses due to the presence of trees; surface heat variations; and turbulent heat transport. Further details of FAST3D-CT are omitted here for brevity but are available in the literature.^{12,13}

An efficient methodology is available to generate the requisite terrain geometry for FAST3D-CT. High-resolution (1 m or smaller) vector geometry data are commercially available for most major cities. From these data, several downtown urban landscapes have been modeled and generated, such as Baghdad, Iraq; Chicago, Illinois; Los Angeles, California; New York City, New York; Oklahoma City, Oklahoma; and Washington, DC.⁴ Environment–vehicle interaction results presented within the APL UAS mission planning and simulation tool are for a simulated trajectory through downtown Baghdad with the appropriate MILES FAST3D-CT urban airflow model.

Validation of these urban and complex terrain airflow LES computations has been performed on a limited basis. Detailed time-dependent wind field observations at various locations can be, at the least, used for global validation. However, for full validation, the number of field observations may be too numerous and time prohibitive, rendering this an impossible task. For the downtown airflow computations of Oklahoma City, a three-way validation was performed using field trial data, wind tunnel simulations, and detailed time-dependent computations using the MILES FAST3D-CT model. Direct comparisons with field data [e.g., the 2003 Joint Urban field trial (JU2003) experiments in Oklahoma City^{10,14,15}] provide an intuitively more “believable” validation; however, the scarcity of experimental field trial data makes more quantitative validation difficult.

Wind tunnel comparisons allow more rigorous validation, but, until recently, typical available data insufficiently characterized the coherent structures. From recent research efforts involving the U.S. Naval Research Laboratory and the University of Hamburg, a comprehensive set of validation data for urban flow modeling has been compiled. Detailed comparisons with wind tunnel test measurements and contaminant transport computations over an accurate urban model of Oklahoma City were conducted to evaluate and validate the ability of FAST3D-CT to model the urban airflow.¹⁶ Figure 4 shows a section of the downtown Oklahoma City model being put in place at the University of Hamburg wind tunnel test section.

Vertical velocity profiles for both the wind tunnel test and computational models were taken at numerous locations within a downtown area and at a wider spacing along the outer downtown area edges. The airflow



Figure 4. View of the 4 × 3 m test section at the University of Hamburg wind tunnel as a section of the Oklahoma City model is being put in place. A turntable is used to allow consideration of different wind directions. The scale is 1:300. (Reprinted from Ref. 7 with permission of the American Institute of Aeronautics and Astronautics.)

was analyzed for six different wind directions. Wind tunnel vertical velocity profile measurements were done at scaled heights representing distances between 6 and 260 m above ground at full scale. A time series of the translational wind velocity components (u_{wind} , v_{wind} , w_{wind}) was obtained at each height for the vertical velocity profile. For the MILES FAST3D-CT computations, data were extracted along the same vertical profile locations and compared with the wind tunnel test results. As an example, Fig. 5 shows a comparison, for a prevailing southerly wind, of the mean wind velocity (u -direction velocity component) at four vertical profiles along Robinson Avenue in downtown Oklahoma City. This comparison shows agreement, at worst, to within $\pm 10\%$, which is within the measurement uncertainty. In general, very good agreement between the MILES FAST3D-CT computations, wind tunnel data, and the field trial results has been obtained.

Although agreement could presumably be improved with better calibration of the unsteady component of the prescribed inflow conditions, this calibration is very difficult because it must be based on laboratory (or field) databases, which typically provide single-point statistics; these statistics are insufficient to characterize the unsteady structure of the flow. However, a particularly valuable insight is that, despite these inherent difficulties in calibrating the inflow boundary conditions, the fluid dynamics deep within the urban model domain, beyond the first one or two street canyons, seems to be insulated by the dynamics and new vortex shedding in the boundary rows of buildings and thus appears to be less dependent on the exact details of the inflow conditions. Overall, validation efforts to date indicate that reasonable agreement can be achieved with benchmark

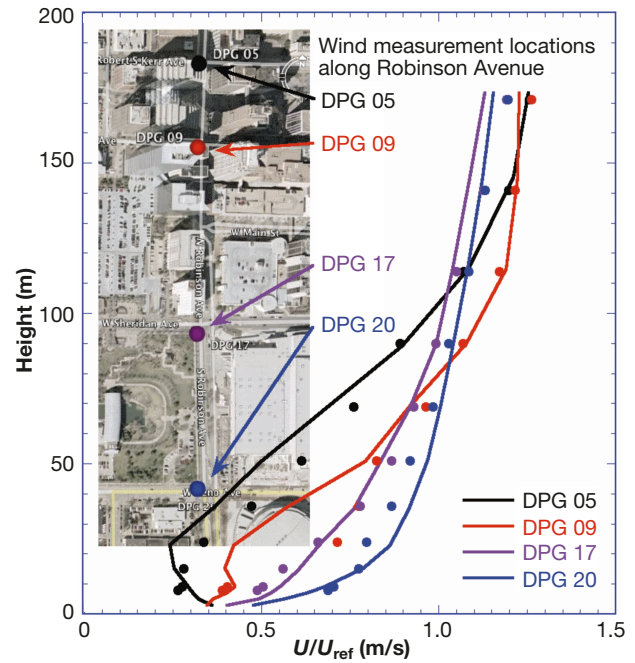


Figure 5. Comparison of wind profiles from wind tunnel measurements (filled circles) and numerical simulations (solid lines) at four locations along Robinson Avenue in downtown Oklahoma City, Oklahoma. Inset shows measurement locations Dugway Proving Ground (DPG) 05, 09, 17, and 20. (Reprinted from Ref. 7 with permission of the American Institute of Aeronautics and Astronautics.)

laboratory data and the current MILES FAST3D-CT models using resolutions achievable and suitable to capture downtown urban landscapes as well as the larger urban environments. Perhaps a more sophisticated and complex validation methodology should be based on a probabilistic approach as performed by Harms et al.¹⁷

UAS Vehicle Dynamics Component

The UAS vehicle dynamics component is a Simulink-based six-degree-of-freedom (6-DOF) motion or trajectory simulation, which was developed to easily emulate the closed-loop flight performance of any fixed-wing air vehicle. The UAS vehicle dynamics component consists of modular elements emulating on-vehicle processing (mission data, guidance, and autopilot response), the UAS physical model (vehicle model), and physics (6-DOF kinematics and environment), as well as onboard sensors (feedback measurements and estimation). External inputs and outputs allow the Simulink simulation to fluidly interface with the overall UAS mission planning and simulation tool, passing vehicle kinematics data out to the overall simulation and inputting mission data as well as wind data from the UAS terrain airflow component. Furthermore, the UAS platform modular element emulates the UAS control surface actuator response, motor, mass properties, and 6-DOF aerodynamics. To accurately simulate the flight, data are

exchanged among three of the five components of the UAS mission planning and simulation tool (unsteady LES terrain airflow, complex terrain, and the UAS vehicle dynamics components).

The 6-DOF simulation solves the equations of motion along some prescribed trajectory as a function of time. The model comprises a set of six equations representing the translational and rotational motion of a body in space and time. In general, the set of equations of motion are listed below.

Translational (force) equations:

$$\begin{aligned} X_A - mg \sin \theta + T &= m(\dot{u} + qw - rv) \\ Y_A + mg \sin \phi \cos \theta &= m(\dot{v} + ru - pw) \\ Z_A + mg \cos \phi \cos \theta &= m(\dot{w} + pv - qu) \end{aligned} \quad (1)$$

Rotational (moment) equations:

$$\begin{aligned} L_A &= I_{xx}\dot{p} - I_{xz}\dot{r} + (I_{zz} - I_{yy})qr - I_{xz}pq \\ M_A &= I_{yy}\dot{q} + (I_{xx} - I_{zz})pr + I_{xz}(p^2 - r^2) \\ N_A &= I_{zz}\dot{r} - I_{zx}\dot{p} + (I_{yy} - I_{xx})pq + I_{xz}qr \end{aligned} \quad (2)$$

In these equations, T , X_A , Y_A , Z_A , L_A , M_A , and N_A represent the vehicle thrust and six aerodynamic forces and moments along the x , y , and z body axes. The vehicle mass properties are the mass (m), the principle mass moments of inertia (I_{xx} , I_{yy} , and I_{zz}), and the cross-product mass moments of inertia (I_{xz} and I_{zx}). In some instances, the cross-product inertial terms may be neglected, but for now these terms are included. Gravity is represented by g , and the vehicle translational and rotational velocities and accelerations are u , v , w , \dot{u} , \dot{v} , \dot{w} , p , q , r , \dot{p} , \dot{q} , \dot{r} . Finally, the vehicle pitch and roll orientation angles,

which are referenced from the local horizontal to the body-axes coordinate system, are θ and ϕ , respectively. In the 6-DOF formulation, the equations are rewritten in terms of the translational $(\dot{u}, \dot{v}, \dot{w})$ and rotational $(\dot{p}, \dot{q}, \dot{r})$ accelerations and then numerically solved by integrating in time to obtain the velocity and position at each succeeding time step. This process is repeated until the desired trajectory has been computed as a function of time.

Understanding the formulation of the equations of motion is important because one can then identify variables within these equations that account for the environment-vehicle interactions. The left-hand side of the equations of motion represents the external forces and moments affecting the vehicle, while the right-hand side represents the vehicle state variables. For the 6-DOF formulation, the aerodynamic forces and moments of the vehicle are determined by looking them up in the UAS aerodynamic database. Likewise, environment-vehicle interactions are determined using a combination of the UAS aerodynamic database, unsteady LES terrain airflow database, and complex terrain components. Furthermore, the environment-vehicle interactions are accounted for by adding increments to either the aerodynamic forces and moments or state variables. Figure 6 shows a block diagram of the implementation of environment-vehicle interaction models in the UAS vehicle dynamics component.

ENVIRONMENT-VEHICLE INTERACTION MODEL DEVELOPMENT

Environment-vehicle interaction models were developed that encompass varying degrees of the physics or functional relationships with the complex terrain environment. Some models are relatively simplistic or are a low-order representation of the interactions, while other models account for the geometric and mass relationship between the environment and vehicle. One model not only captures the geometric and mass relationship but also includes a term for the rotational resistance due to aerodynamic damping. Some aspects of each interaction model may require additional consideration and further work to verify and validate these models.

As previously stated, the environment-vehicle interactions can be accounted for by incre-

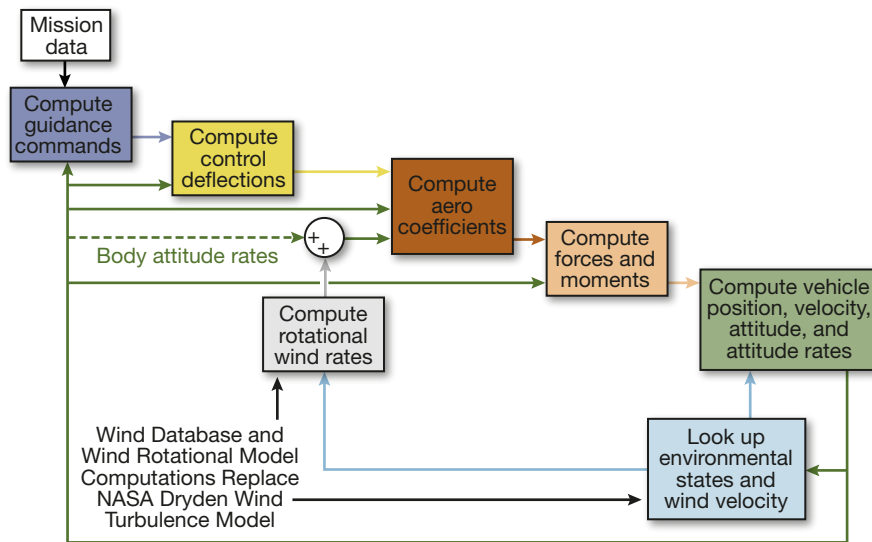


Figure 6. Block diagram of the implementation of environment-vehicle interaction models in the UAS vehicle dynamics component of the mission planning and simulation tool.

ments to either the aerodynamic forces and moments or state variables. In this formulation, the interaction models can be classified into two distinct types, coefficient-based and rate-based. Both model types are represented as the superposition of a steady and unsteady contribution and are shown in equation form below.

Coefficient-based model:

$$\begin{aligned}
 \text{Drag Force Coefficient: } C'_D &= C_{D_{steady}} + C_{D_{unsteady}} \\
 \text{Side Force Coefficient: } C'_Y &= C_{Y_{steady}} + C_{Y_{unsteady}} \\
 \text{Lift Force Coefficient: } C'_L &= C_{L_{steady}} + C_{L_{unsteady}} \\
 \text{Rolling Moment Coefficient: } C'_l &= C_{l_{steady}} + C_{l_{unsteady}} \\
 \text{Pitching Moment Coefficient: } C'_m &= C_{m_{steady}} + C_{m_{unsteady}} \\
 \text{Yawing Moment Coefficient: } C'_n &= C_{n_{steady}} + C_{n_{unsteady}}
 \end{aligned} \tag{3}$$

Rate-based model:

$$\begin{aligned}
 \text{x-axis Translational Velocity: } u' &= u_{steady} + u_{unsteady} \\
 \text{y-axis Translational Velocity: } v' &= v_{steady} + v_{unsteady} \\
 \text{z-axis Translational Velocity: } w' &= w_{steady} + w_{unsteady} \\
 \text{x-axis Rotational Velocity: } p' &= p_{steady} + p_{unsteady} \\
 \text{y-axis Rotational Velocity: } q' &= q_{steady} + q_{unsteady} \\
 \text{z-axis Rotational Velocity: } r' &= r_{steady} + r_{unsteady}
 \end{aligned} \tag{4}$$

The 6-DOF simulation computes trajectories through a complex environment, such as Oklahoma City or Baghdad. Three other M&S framework components—the UAS aerodynamic database, unsteady LES terrain airflow database, and complex terrain components—are used by the 6-DOF simulation. Information from all three of these components along the trajectory is used to estimate the steady and unsteady terms in both the coefficient- and rate-based model formulations. The steady terms are generally computed using the mean or nominal flight conditions, while the unsteady terms are computed using the environment–vehicle interaction models.

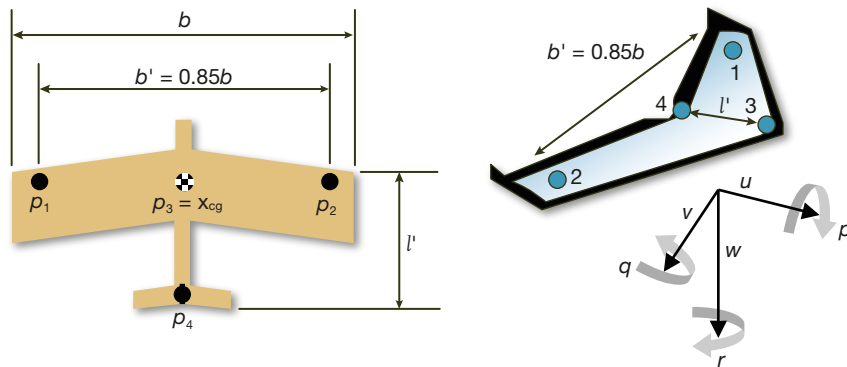


Figure 7. Definition of vehicle reference points for the coefficient- and rate-based models. (Adapted from Ref. 7 with permission of the American Institute of Aeronautics and Astronautics.)

Both model types must use database information referenced to the vehicle center of gravity, \bar{x}_{cg} . However, additional geometrical information relative to \bar{x}_{cg} is needed by the interaction models. Both the coefficient- and rate-based models use a set of at least four vehicle body points for which database information is needed. Figure 7 shows an illustration defining the geometric locations of these body vehicle points, p_1 , p_2 , p_3 , and p_4 . Although four body vehicle points are defined here, an extension of the coefficient- or rate-based model formulation may incorporate a finer discretization in both the lateral and longitudinal directions. As will be shown later, information from the databases is used to compute the linear and rotational wind velocity components at these vehicle body points relative to the time and position along some trajectory within the complex terrain environment. This information includes local flow angles (angles of attack and sideslip, α and β) and increments relative to the nominal flow angles at each of these points.

For the coefficient-based models, the interaction effects both in translation and rotation are accounted for in the incremental unsteady force and moment coefficients, respectively. For the rate-based models, translation is simply accounted for by adding wind velocity increments to the vehicle velocity, and rotation is accounted for by adding wind angular velocity increments to the vehicle angular velocity. In other words, the coefficient-based model formulation includes both the translational and rotational increments, whereas the rate-based model formulation only includes the rotational increments. In the rate-based formulation, there is no need to develop a model for translation increments because they are accounted for in the translational velocity definition.

Development of these interaction models addresses the need to understand the time-varying airflow and its impact on vehicle performance. These interaction models encompass many of the necessary geometrical and physics-based functional relationships. In the model formulation,

no assumptions are made that restrict application of these interaction models to a specific urban or complex terrain environment. In fact, application to other environments appears to be valid, although it has not yet been validated and verified. A more detailed presentation of the interaction model formulation is given in Ref. 18.

Coefficient-Based Modeling Formulation

Typically, contributions of the various vehicle aerodynamic forces

and moments are assumed constant or steady at any instance in time, but for unsteady environment–vehicle interaction modeling, this assumption is modified to include a time-dependent contribution. The vehicle aerodynamic forces and moments are represented as the superposition of both steady and unsteady contributions as represented in Eq. 3. The unsteady contribution is the interaction between the vehicle and the winds within the urban or complex terrain environment. The coefficient-based model makes use of a series expansion of the force and moment coefficients for both the steady and unsteady contributions as a function of the various flight parameters. One such series expansion for the drag coefficient is given as follows:

$$C_D = C_{D_0} + C_{D_\alpha} \alpha + C_{D_{\dot{\alpha}}} \left(\frac{\dot{\alpha} \bar{c}}{2V} \right) + C_{D_\beta} \beta + C_{D_{\dot{\beta}}} \left(\frac{\dot{\beta} \bar{c}}{2V} \right) + C_{D_q} \left(\frac{q \bar{c}}{2V} \right) + C_{D_{\delta_a}} \delta_a + C_{D_{\delta_e}} \delta_e + C_{D_{\delta_f}} \delta_f + C_{D_{\delta_r}}, \quad (5)$$

where C_{D_0} , C_{D_α} , $C_{D_{\dot{\alpha}}}$, C_{D_β} , $C_{D_{\dot{\beta}}}$, C_{D_q} , $C_{D_{\delta_a}}$, $C_{D_{\delta_e}}$, $C_{D_{\delta_f}}$, and $C_{D_{\delta_r}}$ are the zero-lift drag, increments in drag due to changes in α , $\dot{\alpha}$, β , $\dot{\beta}$, q , aileron deflection (δ_a), elevator deflection (δ_e), flap deflection (δ_f), and rudder deflection (δ_r), free-stream velocity (V), and reference length (\bar{c}). Similar series expansions not shown can also be given for the other force and moment coefficients. For the steady contribution, the forces and moments are computed using the nominal flow conditions referenced to the vehicle \bar{x}_{cg} . However, for the unsteady contribution, it will be necessary to compute differential contributions to the forces and moments either in the longitudinal and/or lateral directions at the vehicle body point locations. To accomplish this, the series expansions of the force and moment coefficients are simplified to represent only the unsteady contribution. Referring as an example to Eq. 5 and assuming that the unsteady contribution is only a function of α and β , the other terms in Eq. 5 dependent on the rates and control deflections are neglected. The differential flow angles ($\Delta\alpha$ and $\Delta\beta$) between the vehicle reference location, \bar{x}_{cg} , and vehicle body points are computed. The unsteady contribution is the summation of the respective differential terms for the forces and moments at each vehicle body point. Thus, the unsteady contribution is represented as follows:

$$\begin{aligned} C_{D_{unsteady}} &= \Delta C_{D_{p_1}} + \Delta C_{D_{p_2}} = C_{D_\alpha} (\Delta\alpha_{p_1} + \Delta\alpha_{p_2}) + C_{D_\beta} (\Delta\beta_{p_1} + \Delta\beta_{p_2}), \\ C_{Y_{unsteady}} &= \Delta C_{Y_{p_1}} + \Delta C_{Y_{p_2}} = C_{Y_\alpha} (\Delta\alpha_{p_1} + \Delta\alpha_{p_2}) + C_{Y_\beta} (\Delta\beta_{p_1} + \Delta\beta_{p_2}), \\ C_{L_{unsteady}} &= \Delta C_{L_{p_1}} + \Delta C_{L_{p_2}} = C_{L_\alpha} (\Delta\alpha_{p_1} + \Delta\alpha_{p_2}) + C_{L_\beta} (\Delta\beta_{p_1} + \Delta\beta_{p_2}), \\ C_{l_{unsteady}} &= \Delta C_{l_{p_1}} + \Delta C_{l_{p_2}} = C_{l_\alpha} (\Delta\alpha_{p_1} + \Delta\alpha_{p_2}) + C_{l_\beta} (\Delta\beta_{p_1} + \Delta\beta_{p_2}), \\ C_{m_{unsteady}} &= \Delta C_{m_{p_1}} + \Delta C_{m_{p_2}} = C_{m_\alpha} (\Delta\alpha_{p_1} + \Delta\alpha_{p_2}) + C_{m_\beta} (\Delta\beta_{p_1} + \Delta\beta_{p_2}), \\ C_{n_{unsteady}} &= \Delta C_{n_{p_1}} + \Delta C_{n_{p_2}} = C_{n_\alpha} (\Delta\alpha_{p_1} + \Delta\alpha_{p_2}) + C_{n_\beta} (\Delta\beta_{p_1} + \Delta\beta_{p_2}). \end{aligned} \quad (6)$$

In the formulation shown in Eq. 6, only vehicle body points p_1 and p_2 are assumed, for simplicity, to contribute to the unsteady term. Note that other vehicle body points can be contributors as well; for the initial development of the coefficient-based model, other vehicle body point contributions are ignored. Thus, the overall process of computing the steady and unsteady contributions to the forces and moments occurs using Eqs. 5 and 6 in the integration of the equations of motion at a given instance in time and position along the trajectory in complex terrain environment.

Alternate coefficient-based formulations can also be considered. One such alternate formulation is to define the coefficient series expansion in terms of the UAS vehicle component contributions, such as the fuselage, wing, vertical and horizontal tails, and/or control surfaces. With this alternate series expansion, interactions associated with the wing or control surfaces can be isolated.

Rate-Based Modeling Formulation

The rate-based model is the representation of the unsteady environment–vehicle interaction through increments to the vehicle rotational or angular velocity. The genesis of this formulation came from the notion to replace the Dryden wind turbulence model^{19–21} with one that provides an alternate model of the wind angular velocity imparted onto the vehicle. The rate-based model does not consider potential unsteady effects due to thrust or control surface variation but focuses on the angular velocity and/or angular momentum imparted onto the vehicle due to the wind. Equation 4 shows steady and unsteady contributions to the translational and rotational velocities. Estimation of the unsteady angular velocity due to the wind is the focus of the rate-based model development. The complexity of the rate-based formulation is illustrated by understanding that such a relationship should be a function of the wind angular velocity, vehicle geometry, and mass properties. Currently, there are four different rate-based model formulations. The following subsections provide a brief discussion of each model formulation.

Velocity Point Model

For the velocity point model, the vehicle body points (Fig. 7) are tracked as a function of position and time along the vehicle trajectory. Determination of the unsteady or wind angular velocity at each body point is obtained via an interpola-

tion scheme using the terrain airflow database and the relative position within the terrain itself. By defining a geometric relationship between each body point relative to the vehicle \vec{x}_{cg} , estimates of wind angular velocity are computed using the wind translational velocity in the airflow database. This model assumes that the entire magnitude of wind angular velocity is imparted onto the vehicle. Similar applications of the velocity point model are found in the literature.^{22,23} The following equations are used to compute the unsteady roll, pitch, and yaw angular velocities:

$$\begin{aligned} p_{unsteady} &= \frac{(w_2 - w_1)}{b'}, \\ q_{unsteady} &= \frac{(w_4 - w_3)}{l'}, \\ r_{unsteady} &= \frac{(u_1 - u_2)}{b'} \text{ and/or } r_{unsteady} = \frac{(v_3 - v_4)}{l'}. \end{aligned} \quad (7)$$

This is a relatively low-order model formulation that accounts for only a geometric relationship between the environment and vehicle. An alternate form of this model expands the number of body points along the lateral and longitudinal directions, which can capture nonlinear effects due to vehicle geometry or localized wind variations.

Angular Velocity Point Model

The angular velocity point model is similar in concept to the velocity point model, but the wind angular velocity is computed exclusively from the terrain airflow database. Definition of the angular velocity, $\vec{\omega}$, is given in Eq. 8, which is then numerically computed in the entire terrain airflow database using a finite differencing scheme:

$$\vec{\omega} = \frac{1}{2} \text{Vorticity} = \frac{1}{2} \text{curl} \vec{V} = \frac{1}{2} \vec{\nabla} \times \vec{V}. \quad (8)$$

The angular velocity point model is implemented by using a single point or multiple body points. The following is an example of implementation of both a single-point and a four-point angular velocity point model. Again, this model formulation assumes that the entire magnitude of wind angular velocity is imparted to the vehicle.

In the single-point estimation, the body point location coincides with the vehicle center of gravity, \vec{x}_{cg} . The value of the wind angular velocity is extracted from the terrain airflow database by interpolating in time and position relative to the vehicle \vec{x}_{cg} . Thus, the unsteady contribution is given by Eq. 8 evaluated at \vec{x}_{cg} .

In the four-point estimation, the body point locations coincide with the vehicle body point definitions in Fig. 7. As before, the values of the wind angular velocity are interpolated from the terrain airflow database. Then, the unsteady contribution is an average of the angular velocity at the four body points as shown in Eq. 9:

$$\vec{\omega}_{unsteady} = (\vec{\omega}_{p_1} + \vec{\omega}_{p_2} + \vec{\omega}_{p_3} + \vec{\omega}_{p_4}) / 4. \quad (9)$$

An alternative average for the angular velocity is to use subsets of the angular velocities at each of the four body points. Equation 10 shows one such alternative estimation for the unsteady angular velocities for roll, pitch, and yaw:

$$\begin{aligned} p_{unsteady} &= \frac{(p_{p_1} + p_{p_2})}{2}, \\ q_{unsteady} &= \frac{(q_{p_3} + q_{p_4})}{2}, \\ r_{unsteady} &= \frac{(r_{p_3} + r_{p_4})}{2}. \end{aligned} \quad (10)$$

The application of the angular velocity point model assumes a linear variation of the wind velocity along the vehicle lateral and longitudinal directions. This model can be expanded to include multiple body points along the vehicle lateral and longitudinal directions to capture nonlinear variations of the wind angular velocities. Both point models assume that the wind rotational effects are fully imparted to the vehicle. An adaptation to both point models includes a scaling factor that accounts for only a portion of the wind angular velocity imparted onto the vehicle. Such a scaling relationship is shown in Eq. 11,

$$\vec{\omega}'_{unsteady} = f_w \vec{\omega}_{unsteady}, \quad (11)$$

where $0 < f_w \leq 1$.

Angular Momentum Model One

The angular momentum models are based on concepts presented in Ref. 24 in which the wind angular momentum is computed in a surrounding influencing volume around the vehicle and imparted to the vehicle. The angular momentum about the vehicle \vec{x}_{cg} and the time rate of change of the angular momentum or moment about \vec{x}_{cg} are defined by

$$\vec{L} = \vec{r} \times \vec{p} = \vec{r} \times m\vec{V} = \vec{I}\vec{\omega}, \text{ and} \quad (12)$$

$$\frac{d\vec{L}}{dt} = \vec{M} = \vec{I}\dot{\vec{\omega}} + (\vec{\omega} \times \vec{I}\vec{\omega}) \approx \vec{I}\dot{\vec{\omega}}. \quad (13)$$

For the first of the two angular momentum models, Eq. 12 is rewritten to solve for the angular velocity:

$$\vec{\omega} = \vec{I}^{-1}\vec{L} = \vec{I}^{-1}(\vec{r} \times m\vec{V}). \quad (14)$$

The terms on the right-hand side of Eq. 14 are defined as follows: \vec{I} is the vehicle mass moment of inertia matrix; and $\vec{r} \times m\vec{V}$ is the cross product of the position vector, relative to the \vec{x}_{cg} , for a particle in space and its linear momentum vector.

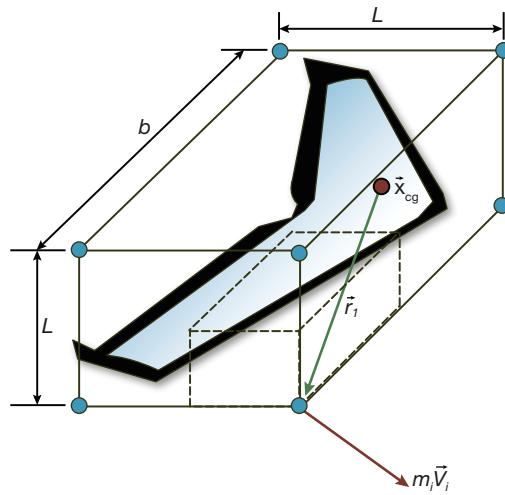


Figure 8. Surrounding influencing volume for the rate-based, angular momentum models. (Adapted from Ref. 7 with permission of the American Institute of Aeronautics and Astronautics.)

The basic concept for this model is that the surrounding influencing volume can be subdivided into smaller subvolumes, where the cross product is computed for each subvolume and then summed to obtain the unsteady environment–vehicle interaction. For the surrounding volume, one assumes the volume is constant, has uniform air density, and surrounds the vehicle. The shape of the surrounding volume can be any desired shape, such as a rectangular parallelepiped, cylinder, or sphere. The shape chosen here is a rectangular parallelepiped. The angular momentum enclosed by the surrounding volume is computed about the vehicle \bar{x}_{cg} . The surrounding volume is subdivided into eight subvolumes. The eight corner points of the larger volume represent the volume control points at which the angular momentum of the air will be computed and assumed to act (see Fig. 8). Equation 15 represents the angular momentum within the surrounding influencing volume:

$$\bar{L}_{wind} = \sum_{i=1}^{i=8} \bar{r}_i \times m_i \bar{V}_i. \quad (15)$$

Putting the result from Eq. 15 and the mass moment of inertia matrix for the vehicle into Eq. 14 gives the final form, Eq. 16, needed to compute the unsteady or wind angular velocity contribution about the vehicle \bar{x}_{cg} :

$$\bar{\omega}_{unsteady} = \begin{Bmatrix} p_{unsteady} \\ q_{unsteady} \\ r_{unsteady} \end{Bmatrix} = \begin{bmatrix} I_{xx} & 0 & 0 \\ 0 & I_{yy} & 0 \\ 0 & 0 & I_{zz} \end{bmatrix}^{-1} \left\{ \sum_{i=1}^{i=8} \bar{r}_i \times m_i \bar{V}_i \right\}. \quad (16)$$

Angular Momentum Model Two

The second angular momentum model starts with Eq. 13, which is rewritten to solve for the angular acceleration:

$$\dot{\bar{\omega}} = \bar{I}^{-1} \bar{M} = \bar{I}^{-1} \frac{d\bar{L}}{dt} = \bar{I}^{-1} \frac{d(\bar{r} \times m\bar{V})}{dt}. \quad (17)$$

The terms on the right-hand side of Eq. 17 are similar to those obtained previously for Eq. 14, but now the second term is the time rate of change of the angular momentum, $\frac{d\bar{L}}{dt}$. The vehicle mass moment of inertia matrix is assumed to be constant; thus, the time rate of change for this quantity is zero. Equation 17 represents the basic formulation of this angular momentum model.

This second angular momentum model uses the complete formulation from the first angular momentum model but incorporates an additional computation for the time rate of change of the angular momentum. To compute the time rate of change of the angular momentum, the angular momentum from the previous time step is needed. This requires the UAS vehicle dynamics component to save computed data at the previous time step. A backward finite differencing scheme is implemented to compute the time rate of change of the angular momentum within the surrounding volume. Equation 18 shows a backward difference representation for the time rate of change of the angular momentum:

$$\frac{d\vec{L}_{unsteady}}{dt} = \frac{\vec{L}_{unsteady}^t - \vec{L}_{unsteady}^{t-\Delta t}}{\Delta t} = \frac{\left\{ \sum_{i=1}^{i=8} r_i \times m_i V_i \right\}^t - \left\{ \sum_{i=1}^{i=8} r_i \times m_i V_i \right\}^{t-\Delta t}}{\Delta t}. \quad (18)$$

The time rate of change of the angular momentum also corresponds to the moment, \vec{M} , about the vehicle \vec{x}_{cg} . In effect, this is the contribution to the aerodynamic moment due to the unsteady or environment-vehicle interaction about the vehicle \vec{x}_{cg} , $\vec{M}_{unsteady} = \frac{d\vec{L}_{unsteady}}{dt}$.

Substituting Eq. 18 into Eq. 17 results in the following expression for the unsteady angular acceleration:

$$\dot{\vec{\omega}}_{unsteady} = \bar{I}^{-1} \left(\frac{d\vec{L}_{unsteady}}{dt} \right) = \bar{I}^{-1} \frac{\left\{ \sum_{i=1}^{i=8} r_i \times m_i V_i \right\}^t - \left\{ \sum_{i=1}^{i=8} r_i \times m_i V_i \right\}^{t-\Delta t}}{\Delta t}. \quad (19)$$

The final step in obtaining the unsteady angular velocity is to integrate Eq. 19 in time.

$$\vec{\omega}_{unsteady} = \int \dot{\vec{\omega}}_{unsteady} dt = \begin{Bmatrix} p_{unsteady} \\ q_{unsteady} \\ r_{unsteady} \end{Bmatrix} = \begin{Bmatrix} \int \dot{p}_{unsteady} dt \\ \int \dot{q}_{unsteady} dt \\ \int \dot{r}_{unsteady} dt \end{Bmatrix}. \quad (20)$$

Modeling Summary

Although these interaction models have yet to be validated with experimental or test data, in the absence of such validation, we can still make considerable progress in examining the effects of these response models in the context of validated far-field terrain airflow models in operationally realistic environments with relevant operational constraints. The UAS mission planning and simulation tool provides exactly the kind of environment in which to perform these studies. Initial efforts have focused on the computational implementation of the coefficient- or rate-based model formulations. These models represent a unique capability with which the environment-vehicle interactions are predicted without the need for a statistical representation of the airflow or wind environment, which is needed in the Dryden wind turbulence model. Currently, only one of the aforementioned environment-vehicle interaction models is integrated into the UAS vehicle dynamics component—the velocity point model.

The original intent of this model development was for application in the urban environment. However, these models are not restricted to only the urban environment. As long as there is an adequate definition of the terrain airflow environment, application of these models is valid for that flight environment. The successful development, implementation, and validation of these environment-vehicle interaction models will help enable an end-to-end mission planning and simulation

capability that is unique in design and potential utility in all aspects of small UAS systems engineering.

TRAJECTORY SIMULATION RESULTS

Trajectory simulation results have been obtained for a notional mission in the downtown area of Baghdad, Iraq. The UAS used for this notional mission is the Unicorn made by Procerus Technologies. The Procerus Unicorn planform is 46 in. from wingtip to wingtip. Figure 9 shows an illustration of the Procerus Unicorn planform shape and the flight path through a portion of downtown Baghdad. Winds for the notional mission were from 020° at 3 m/s (5.8 knots). In Fig. 9, the red curve represents the desired trajectory defined by a set of waypoints. The blue curve represents the simulated trajectory flown with calm winds. The trajectory route starts over the Tigris River southeast of the Al-Jumhuriyah (Republic) Bridge (latitude 33.319° north and longitude 44.410° east). The mission route begins by proceeding in a northeast direction until reaching Saadun Street, where the route then turns to the northwest following Saadun Street through Al-Tahrir Square to Al-Kalany Square. Once reaching Al-Kalany Square, the route turns toward the southwest and proceeds over the Al-Sinak Bridge. At a point about halfway across the Al-Sinak Bridge, a looping left-hand turn is made in order to return to the starting point by retracting the same route back to the starting location.

Three different trajectory simulations are flown



Figure 9. Illustration of the Procerus Unicorn UAS and the notional mission route through downtown Baghdad with winds from 020° at 3 m/s. (Adapted from Ref. 7 with permission of the American Institute of Aeronautics and Astronautics.)

along this route: the first case is with the calm winds; the second case is with the winds from 020° at 3 m/s with only the translational wind velocities included; and the third case is with the winds from 020° at 3 m/s with both the translational and rotational wind velocities included. The fundamental trajectory characteristics that can be examined are the interaction model effects on vehicle trajectory location and position in terms of latitude, longitude, and altitude. Other characteristics include vehicle attitude, angular velocity, and autopilot control commands.

Figure 10 shows the plot of latitude and longitude of the UAS along the notional mission route described above. The first observation to note is that even with calm winds, the UAS does not fly directly through all the waypoints. This is as expected; because the UAS is unable to turn instantaneously as it passes through each waypoint, the UAS autopilot begins maneuvering prior to reaching each waypoint in order to fly toward the next waypoint. The second observation is that the

winds can significantly influence the position of the vehicle throughout the trajectory. It is most apparent when the vehicle is making the looping turn to begin its return leg along the mission route. The winds clearly push the vehicle in a southwest direction relative to the waypoints and in the direction in which the wind is blowing. The third observation is that the velocity point interaction model produces a relatively minor effect on the mission trajectory. For this relatively light breeze, one would probably not expect a significant effect.

Figure 11 shows the vehicle altitude as a function of time along the notional mission route. In general, the altitude varies as a function of time along the mission route in a parabolic manner, where the maximum altitude is at the beginning and end points of the mission route and the minimum altitude occurs around the mission midpoint over the Al-Sinak Bridge. In calm winds, the vehicle descends and climbs in a nearly stair-step fashion along the mission route as commanded by the autopilot. However, once the translational and rotational winds effects are included, the commanded altitude becomes much more difficult to maintain along the mission route. The key observation from this figure is that the translational wind effects are the primary cause for the large variations in vehicle altitude. Inclusion of the rotational

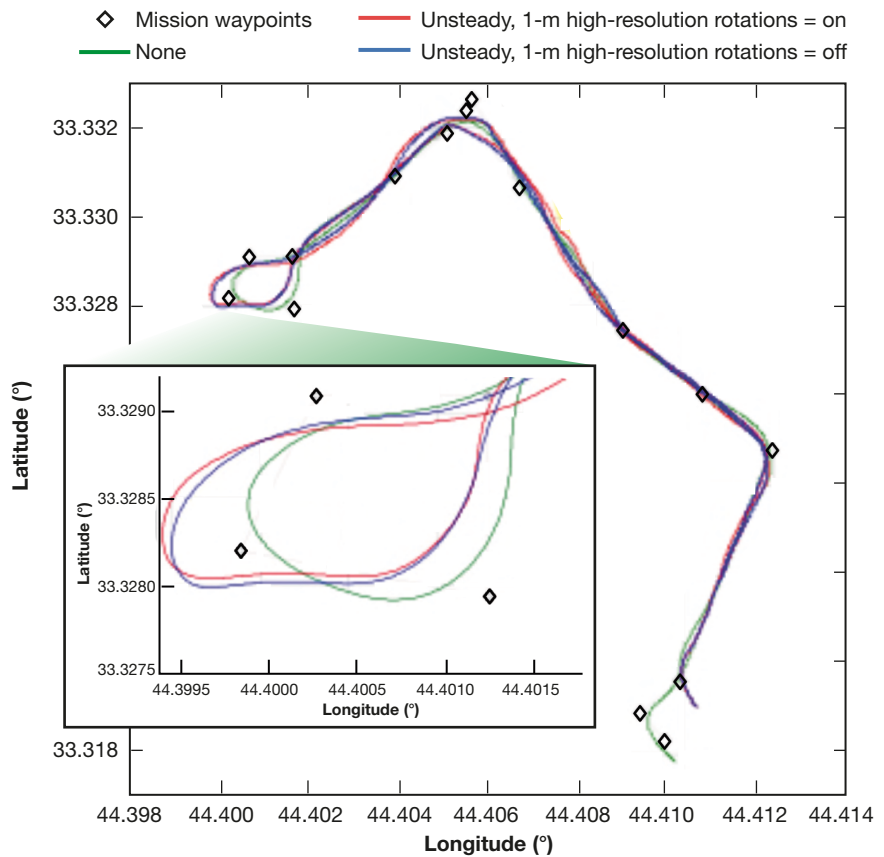


Figure 10. Latitude/longitude of the UAS along the notional mission route in downtown Baghdad for the three different wind condition cases. Latitude/longitude, full, wind decouple = off, rotations = on/off, gain = 3.0, time offset = 67 s.

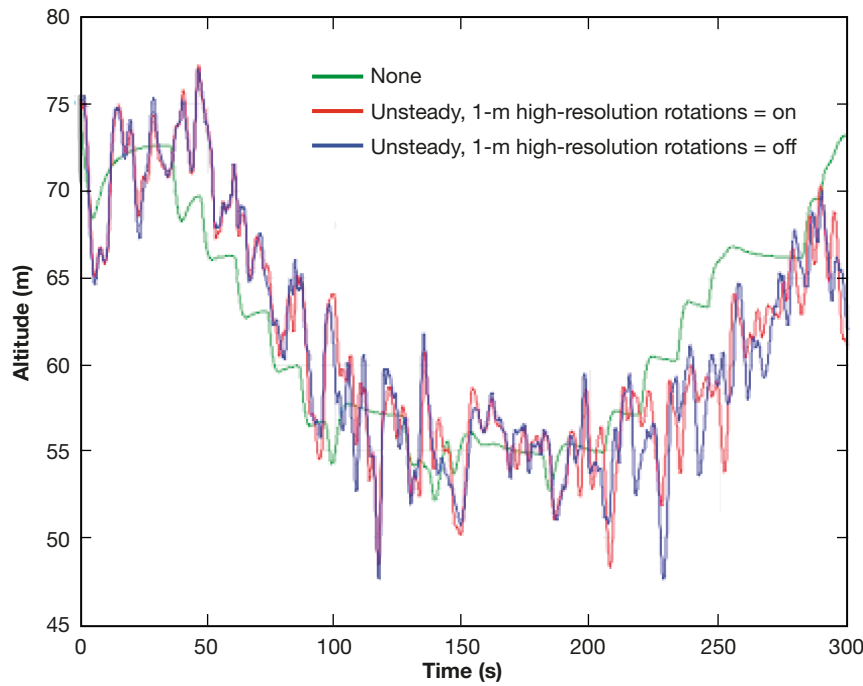


Figure 11. UAS altitude as a function of time along the notional mission route in downtown Baghdad. Altitude, wind decouple = off, rotations = on/off, gain = 3.0, time offset = 67 s.

wind effects appears to induce much smaller variations in altitude. As previously discussed, these results are for a relatively light breeze, but examination at higher wind speeds is necessary to fully understand and characterize the interaction model effects. Variations in vehicle altitude due to the winds appear to be on the order of ± 5 m (16.4 ft). For a vehicle the size of the Procerus Unicorn, this is a significant variation in altitude. Vehicle altitude variations as a function of wind speed are important to characterize; mission planners can use this information to schedule altitudes commanded by the autopilot to have sufficient margin that ensures mission success. Examination of other trajectory simulation results may yield additional information and insight into the interaction model effects as well as rules of thumb valuable to training and/or mission planning.

Figure 12 shows the vehicle attitude angles (roll, pitch, and yaw) as a function of time along the notional mission route. Again, the most apparent effect is the difference between the calm winds and light breeze

conditions. With the winds effects included, all vehicle attitude angles are more oscillatory as a function of time. The most predominant influence on the vehicle attitude appears to come from the translational component of the wind and not the rotational component. However, at certain instances in time along the mission route, the rotational wind components appear to have a large effect. This presumably indicates when and where along the route the vehicle encounters the most turbulent airflow. The vehicle is probably encountering turbulent or vortical airflow structures characteristic of the urban environment (Fig. 1) as described in the *Introduction* and *Unsteady LES Terrain Airflow Database and Complex Terrain Components* sections of this article. A final observation is that

there appears to be a time shift in the data with respect to the calm winds and light breeze conditions. This time shift is expected because the vehicle is flying into (headwind) or with the wind (tailwind), which inhibits or assists the vehicle as it progresses along the mission route. Furthermore, one observes a significant increase

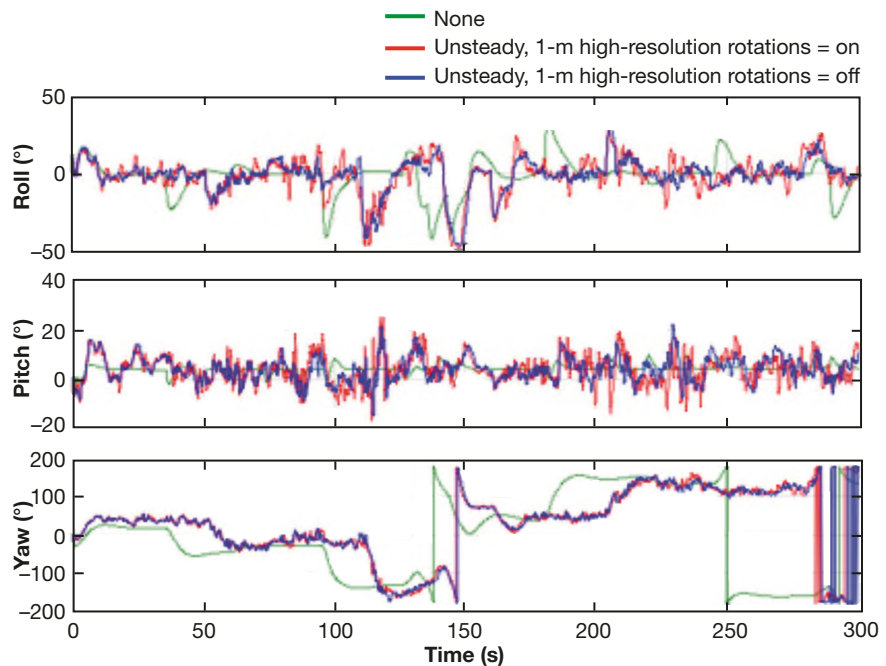


Figure 12. UAS attitude angles as a function of time along the notional mission route in downtown Baghdad. Altitude, wind decouple = off, rotations = on/off, gain = 3.0, time offset = 67 s.

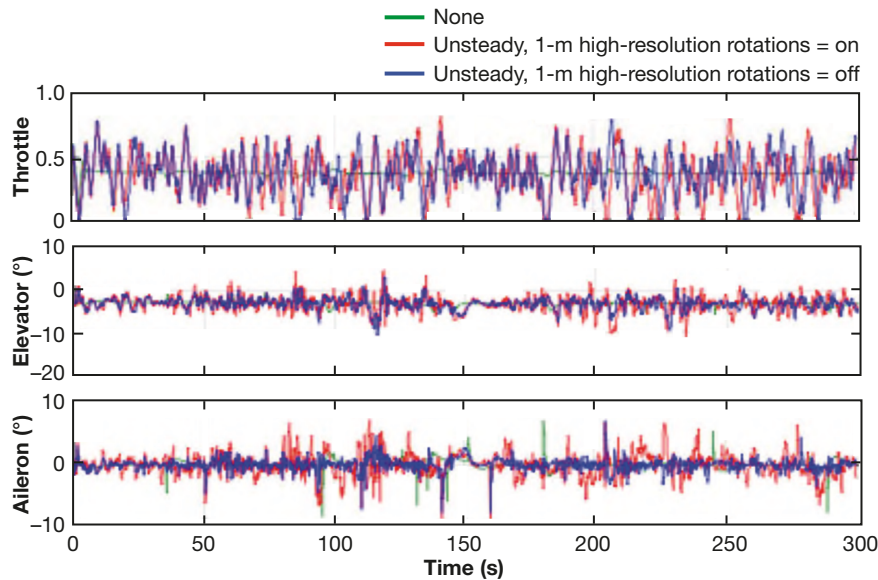


Figure 13. UAS autopilot controls as a function of time along the notional mission route in downtown Baghdad. Altitude, wind decouple = off, rotations = on/off, gain = 3.0, time offset = 67 s.

in the variability in the vehicle attitude angles as the interaction effects are introduced. The variability is as large as $\pm 10^\circ$ in the roll, pitch, and yaw angles. These large variations need to be accounted for in the autopilot design in order to maintain and, if necessary, recover vehicle control.

Figure 13 shows the vehicle autopilot controls as a function of time along the notional mission route. For the calm winds, the vehicle autopilot commands a relatively constant value for each of the throttle, elevator, and aileron settings. But for the light breeze conditions, the autopilot is continually varying the commanded control settings. Clearly, this is an effect of the wind; for the commanded aileron control setting, the largest effect is due to the rotational wind effect, where the frequency and magnitude of the commanded control setting increases significantly compared with just the translational wind effect. This is an as-expected result because the aileron controls the vehicle roll position, which is most affected by changes in the vehicle lift and rolling moment due to the wind. The significance of the variations in the commanded autopilot control settings lies in the required response of the control actuators. Understanding how the control system must be able to respond to the autopilot commands to maintain vehicle control within the urban terrain is critical to the planning and successful execution of UAS missions.

The valuable observations obtained from these notational missions demonstrate the importance of understanding environment–vehicle interactions. These notational missions are by no means a comprehensive study of the interaction effects. To date, only one of the

proposed interaction models has been implemented and assessed. Furthermore, parametric studies are needed to more fully characterize the interaction effects for differences in the wind speed, wind direction, UAS platform parameters, and certain trajectory parameters such as altitude. Such an endeavor could define a set of mission and/or vehicle design parameters for various UAS platforms that would guarantee mission success. The set of mission design and operational parameters would include minimum altitude, minimum and maximum airspeed, vehicle attitude angles limits, maximum wind speed, autopilot command schedules, and geographical “no go” or “stay out” zones. Vehicle design parameters or requirements include control surface

sizing, control actuator sizing and response, autopilot design, and overall vehicle sizing. And finally, if externally mounted, a vehicle’s payload suite should also be considered within the mission design parameter space.

Implementation of these environment–vehicle interaction models into the APL UAS mission planning and simulation tool provides a simulation test bed in which to perform parametric studies to evaluate the mission and vehicle requirements needed to successfully fly missions within the urban and complex terrain environments. Simulation results using the velocity point interaction model provide an excellent example of the airflow and vehicle response characteristics that are critical to understand in order to ensure that UAS missions can be successfully planned and executed within these complex terrains. Implementation of additional interaction models will help further understand the level of physics needed to characterize the vehicle response to the complex terrain airflow, as well as to aid in the design of the vehicle autopilot for mission success.

SUMMARY

This article describes the development of a set of wind interaction models for application in a 6-DOF simulation tool to facilitate the study of environment–vehicle airflow interactions in the complex or urban terrain. Five different models have been developed that fall into two categories, aerodynamic coefficient- and rated-based models. They were developed to numerically quantify the effect unsteady airflow has on the control, stability, and performance of the UAS flying in such complex ter-

rain environments. Furthermore, the physics represented in each interaction model varies, allowing for the assessment of the appropriate level of physics needed to best capture and characterize the interaction effects. Trajectory simulation results have been presented for a flight of the Procerus Unicorn UAS over Baghdad using the velocity point model. The results indicate that perhaps the primary wind effect comes from the translational component and not the rotational component. That is not meant to imply that the rotational wind component is unimportant; the rotational interaction does affect the vehicle response. Examination of the simulation results revealed that the rotational interaction could significantly affect vehicle altitude, attitude, and commanded autopilot controls, particularly in pitch and roll. Results could be used to further define mission planning, operational, and vehicle design parameters to ensure mission success within the complex terrain environment.

Critical to the design and creation of this toolset was, and is, a fundamental focus on the physics. If poor assumptions are made about the nature of flow fields in the complex environments in which we are interested, or if the physics are not properly captured, results from systems engineering analyses will be flawed, mission planning solutions will be inadequate, and training will be unrealistic. Two of the most important, and challenging, aspects of the physics have been focal points in this article: the flow fields in complex environments and the interactions between these flow fields and actual vehicle flight. The resulting toolset—which combines these aspects with all the other elements of this effort to achieve an end-to-end capability—is unique in both its design and its potential utility in all aspects of small UAS systems engineering.

RECOMMENDATIONS

With the successful development of the environment-vehicle interaction models, additional work is still needed to further understand and characterize the dynamic impacts on vehicle stability, control, and performance. First, a more thorough parametric study is needed to examine and characterize the interaction effects. Initially, the study should focus on a single UAS platform and mission route while varying such parameters as wind speed and wind direction. A next step would be to implement additional interaction models and vary the wind parameters in the same fashion for each model. Consideration of both the coefficient- and rate-based modeling formulations is important as well. These studies would help characterize the interaction effects for a specific UAS and mission route, focusing on assessing the various trajectory variables and commanded autopilot control settings. An initial study could also verify the need for different levels of physics represented in the interaction

models. A next step in the parametric process would be to begin varying either the UAS platform or the mission route. Varying the UAS platform would help identify how the interaction effects change with respect to vehicle geometry. Analogously, varying the mission route would help identify changes in the interaction effects due to differences within the terrain and associated airflow. One last variation that could be considered would be to investigate a second urban area other than Baghdad (for example, Oklahoma City, Oklahoma). Information gathered from such parametric studies would provide a wealth of insight into how much and what is most affected by the wind translational and rotational effects, which could then be used to design a more robust autopilot for the complex terrain environments.

A second recommendation is to validate these interaction models. Validation is critical to ensure that these models are indeed properly representing the interaction effects, but in practice it is difficult to accomplish. The difficulties and challenges of successful model validation were pointed out in the *Introduction* section. Computational and experimental methods need to be developed to aid in this validation. Perhaps an incremental approach to validation is needed that uses well-controlled wind scenarios that are pertinent yet easily modeled and replicated. Such scenarios may include both computations and wind tunnel measurements of a well-controlled vertical or lateral wind gust. While only a subset of the interaction models may be exercised with such controlled experiments, prediction confidence could be achieved in a piecemeal fashion. As validation studies are pursued, interaction model development and implementation should continue in parallel. They will yield worthwhile insight into maintaining UAS vehicle stability and control in these complex airflow environments.

ACKNOWLEDGMENTS: We thank Mr. Jonathan C. Castelli and Mr. Erich H. Mueller of the APL Force Projection Department for their efforts in coding and implementing the velocity point model into the UAS vehicle dynamics component of the UAS mission planning and simulation tool. Mr. Castelli also produced the trajectory comparison results of the velocity point model for the downtown Baghdad scenario. Their contributions to the overall UAS M&S efforts are appreciated.

REFERENCES

- ¹U.S. Department of Defense, *Unmanned Systems Integrated Roadmap, FY 2009–2034*, Office of the Secretary of Defense (2009).
- ²U.S. Army, *Eyes of the Army U.S. Army Roadmap for Unmanned Aircraft Systems 2010–2035*, U.S. Army UAS Center of Excellence, Fort Rucker, AL (2010).
- ³Martinuzzi, R., and Tropea, C., “The Flow Around Surface-Mounted, Prismatic Obstacles Placed in a Fully Developed Channel Flow,” *J. Fluids Eng.* 115(1), 85–92 (1993).

- ⁴Fernando, H. J. S., “Fluid Dynamics of Urban Atmospheres in Complex Terrain,” *Annu. Rev. Fluid Mech.* **42**, 365–389 (Jan 2010).
- ⁵Boris, J. P., “Dust in the Wind: Challenges for Urban Aerodynamics,” in *Proc. 35th AIAA Fluid Dynamics Conf. and Exhibit*, Toronto, Ontario, Canada, paper AIAA-2005-5393 (2005).
- ⁶Barton, J. D., Cybyk, B., Drewry, D. G., Frey, T. M., Funk, B. K., et al., “Use of a High-Fidelity UAS Simulation for Design, Testing, Training, and Mission Planning for Operation in Complex Environments,” in *Wiley Encyclopedia of Operations Research and Management Science (EORMS)*, J. J. Cochran (ed.), John Wiley & Sons, Inc., Hoboken, NJ (2011).
- ⁷Cybyk, B. Z., McGrath, B., Frey, T. M., Drewry, D. G., Keane, J. F., and Patnaik, G., “Unsteady Urban Airflows and Their Impact on Small Unmanned Air System Operations,” in *Proc. AIAA Atmospheric Flight Mechanics Conf.*, Chicago, IL, paper AIAA-2009-6049 (2009).
- ⁸Cybyk, B. Z., Boris, J. P., Young, T. R., Emery, M. H., and Cheatham, S. A., “Simulation of Fluid Dynamics Around Complex Urban Geometries,” in *Proc. 39th AIAA Aerospace Sciences Meeting & Exhibit*, Reno, NV, paper AIAA-2001-0803 (2001).
- ⁹Patnaik, G., Boris, J. P., Grinstein, F. F., and Iselin, J. P., “Large Scale Urban Simulations with the MILES Approach,” in *Proc. 16th AIAA Computational Fluid Dynamics Conf.*, Orlando, FL, paper AIAA-2003-4104 (2003).
- ¹⁰Allwine, K. J., Shinn, J. H., Streit, G. E., Clawson, K. L., and Brown, M., “Overview of Urban 2000: A Multiscale Field Study of Dispersion Through an Urban Environment,” *Bull. Am. Meteorol. Soc.* **83**(4), 521–536 (2002).
- ¹¹Grinstein, F. F., and Fureby, C., “From Canonical to Complex Flows: Recent Progress on Monotonically Integrated LES,” *Comput. Sci. Eng.* **6**(2), 37–49 (2004).
- ¹²Patnaik, G., Boris, J. P., Grinstein, F. F., and Iselin, J., “Large Scale Urban Simulations with FCT,” in *High-Resolution Schemes for Convection-Dominated Flows: 30 Years of FCT*, D. Kuzmin, R. Löhner, and S. Turek (eds.), Springer Verlag, Berlin, pp. 105–130 (2005).
- ¹³Patnaik, G., Grinstein, F. F., Boris, J. P., Young, T. R., and Parmhed, O., “Large Scale Urban Simulations,” in *Implicit Large Eddy Simulation: Computing Turbulent Flows*, F. Grinstein, L. Margolin, and W. Rider (eds.), Cambridge University Press, New York, pp. 502–530 (2007).
- ¹⁴Allwine, K. J., and Flaherty, J. E., *Joint Urban 2003: Study Overview and Instrument Locations*, Report PNNL-15967, Pacific Northwest National Laboratory, Richland, WA (Aug 2006).
- ¹⁵Allwine, K. J., Leach, M. J., Stockham, L. W., Shinn, J. S., Hosker, R. P., et al., “Overview of Joint Urban 2003—An Atmospheric Dispersion Study in Oklahoma City,” in *Proc. Symp. on Planning, Nowcasting, and Forecasting in the Urban Zone and Eighth Symp. on Integrated Observing and Assimilation Systems for Atmosphere, Oceans, and Land Surface*, Seattle, WA, paper J7.1 (2004).
- ¹⁶Boris, J., Patnaik, G., Young Lee, M., Young, T., Leitl, B., et al., “Validation of an LES Urban Aerodynamics Model for Homeland Security,” in *Proc. 47th AIAA Aerospace Sciences Meeting Including The New Horizons Forum and Aerospace Exposition*, Orlando, FL, paper AIAA-2009-1633 (2009).
- ¹⁷Harms, F., Leitl, B., Schatzmann, M., and Patnaik, G., “Validating LES-based Flow and Dispersion Models,” *J. Wind Eng. Ind. Aerodyn.* **99**(4), 289–295 (2011).
- ¹⁸McGrath, B. E., “Development of Several Models of the Wind Rotational Effects Imparted onto a UAS in the Urban Environment,” Technical Memorandum GVD-11-0010, JHU/APL, Laurel, MD (Mar 2011).
- ¹⁹The MathWorks Product Help, *MATLAB/Simulink Support Documentation for Aerospace Blockset*, The MathWorks Inc., 2007.
- ²⁰Military Specification, *Flying Qualities of Piloted Airplanes*, MIL-F-8785C (Nov 1980).
- ²¹U.S. Department of Defense Handbook, *Flying Qualities of Piloted Aircraft*, MIL-HDBK-1797 (Dec 1997).
- ²²Galway, D., Etele, J., and Fusina, G., “Modeling of the Urban Gust Environment with Application to Autonomous Flight,” in *Proc. AIAA Atmospheric Flight Mechanics Conf. and Exhibit*, Honolulu, HI, paper AIAA-2008-6565 (2008).
- ²³Holley, W. E., and Bryson, A. E., “Wind Modeling and Lateral Control for Automatic Landing,” *AIAA J. Spacecr. Rockets* **14**(2), 65–72 (1977).
- ²⁴Stewart, E. C., “A Study of the Interaction between a Wake Vortex and an Encountering Airplane,” in *Proc. Atmospheric Flight Mechanics Conf.*, Monterey, CA, paper AIAA-1193-3642 (1993).

The Authors

Brian E. McGrath is a member of the APL Senior Professional Staff in the Aerospace Systems Design Group of the Force Projection Department. During the independent research and development (IR&D) projects that supported this work, he was a team member and technical contributor, as well as a Principal Investigator for the follow-on IR&D project. **Bohdan Z. Cybyk** is a member of APL's Principal Professional Staff and is Chief Engineer of the Precision Engagement Business Area Office in the Force Projection Department. During the IR&D projects that supported this work, he was a Co-Principal Investigator, team member, and technical contributor. **Timothy M. Frey** is a member of APL's Principal Professional Staff and is Group Supervisor of the Awareness and Response Information Systems Group in the Asymmetric Operations Department. During the IR&D projects that supported this work, he was a team member and technical contributor. For further information on the work reported here, contact Brian McGrath. His e-mail address is brian.mcgrath@jhupl.edu.

The Johns Hopkins APL Technical Digest can be accessed electronically at www.jhuapl.edu/techdigest.